Paper pa02-066
Submitted to the 28th International Conference on High Energy Physics
ICHEP'96, Warsaw, Poland, July 1996

DESY 96-023
To be publ. in Nucl. Phys. **B**

Elastic Electroproduction of ϱ and J/ψ Mesons at large Q^2 at HERA

H1 Collaboration

Abstract

The total cross sections for the elastic electroproduction of ϱ and J/ψ mesons for $Q^2 > 8$ GeV^2 and $\langle W \rangle \simeq 90$ GeV/c^2 are measured at HERA with the H1 detector. The measurements are for an integrated electron−proton luminosity of $\simeq 3$ pb^{-1}. The dependences of the total virtual photon−proton ($\gamma^* p$) cross sections on Q^2, W and the momentum transfer squared to the proton (t), and, for the ρ, the dependence on the polar decay angle ($\cos\theta^*$), are presented. The J/ψ : ϱ cross section ratio is determined. The results are discussed in the light of theoretical models and of the interplay of hard and soft physics processes.

S. Aid[14], V. Andreev[26], B. Andrieu[29], R.-D. Appuhn[12], M. Arpagaus[37], A. Babaev[25], J. Bähr[36], J. Bán[18], Y. Ban[28], P. Baranov[26], E. Barrelet[30], R. Barschke[12], W. Bartel[12], M. Barth[5], U. Bassler[30], H.P. Beck[38], H.-J. Behrend[12], A. Belousov[26], Ch. Berger[1], G. Bernardi[30], R. Bernet[37], G. Bertrand-Coremans[5], M. Besançon[10], R. Beyer[12], P. Biddulph[23], P. Bispham[23], J.C. Bizot[28], V. Blobel[14], K. Borras[9], F. Botterweck[5], V. Boudry[29], A. Braemer[15], W. Braunschweig[1], V. Brisson[28], D. Bruncko[18], C. Brune[16], R. Buchholz[12], L. Büngener[14], J. Bürger[12], F.W. Büsser[14], A. Buniatian[12,39], S. Burke[19], M.J. Burton[23], G. Buschhorn[27], A.J. Campbell[12], T. Carli[27], F. Charles[12], M. Charlet[12], D. Clarke[6], A.B. Clegg[19], B. Clerbaux[5], S. Cocks[20], J.G. Contreras[9], C. Cormack[20], J.A. Coughlan[6], A. Courau[28], M.-C. Cousinou[24], G. Cozzika[10], L. Criegee[12], D.G. Cussans[6], J. Cvach[31], S. Dagoret[30], J.B. Dainton[20], W.D. Dau[17], K. Daum[35], M. David[10], C.L. Davis[19], B. Delcourt[28], A. De Roeck[12], E.A. De Wolf[5], M. Dirkmann[9], P. Dixon[19], P. Di Nezza[33], W. Dlugosz[8], C. Dollfus[38], J.D. Dowell[4], H.B. Dreis[2], A. Droutskoi[25], D. Düllmann[14], O. Dünger[14], H. Duhm[13], J. Ebert[35], T.R. Ebert[20], G. Eckerlin[12], V. Efremenko[25], S. Egli[38], R. Eichler[37], F. Eisele[15], E. Eisenhandler[21], R.J. Ellison[23], E. Elsen[12], M. Erdmann[15], W. Erdmann[37], E. Evrard[5], A.B. Fahr[14], L. Favart[5], A. Fedotov[25], D. Feeken[14], R. Felst[12], J. Feltesse[10], J. Ferencei[18], F. Ferrarotto[33], K. Flamm[12], M. Fleischer[9], M. Flieser[27], G. Flügge[2], A. Fomenko[26], B. Fominykh[25], J. Formánek[32], J.M. Foster[23], G. Franke[12], E. Fretwurst[13], E. Gabathuler[20], K. Gabathuler[34], F. Gaede[27], J. Garvey[4], J. Gayler[12], M. Gebauer[36], A. Gellrich[12], H. Genzel[1], R. Gerhards[12], A. Glazov[36], U. Goerlach[12], L. Goerlich[7], N. Gogitidze[26], M. Goldberg[30], D. Goldner[9], K. Golec-Biernat[7], B. Gonzalez-Pineiro[30], I. Gorelov[25], C. Grab[37], H. Grässler[2], R. Grässler[2], T. Greenshaw[20], R. Griffiths[21], G. Grindhammer[27], A. Gruber[27], C. Gruber[17], J. Haack[36], D. Haidt[12], L. Hajduk[7], M. Hampel[1], W.J. Haynes[6], G. Heinzelmann[14], R.C.W. Henderson[19], H. Henschel[36], I. Herynek[31], M.F. Hess[27], W. Hildesheim[12], K.H. Hiller[36], C.D. Hilton[23], J. Hladký[31], K.C. Hoeger[23], M. Höppner[9], D. Hoffmann[12], T. Holtom[20], R. Horisberger[34], V.L. Hudgson[4], M. Hütte[9], H. Hufnagel[15], M. Ibbotson[23], H. Itterbeck[1], A. Jacholkowska[28], C. Jacobsson[22], M. Jaffre[28], J. Janoth[16], T. Jansen[12], L. Jönsson[22], K. Johannsen[14], D.P. Johnson[5], L. Johnson[19], H. Jung[10], P.I.P. Kalmus[21], M. Kander[12], D. Kant[21], R. Kaschowitz[2], U. Kathage[17], J. Katzy[15], H.H. Kaufmann[36], O. Kaufmann[15], S. Kazarian[12], I.R. Kenyon[4], S. Kermiche[24], C. Keuker[1], C. Kiesling[27], M. Klein[36], C. Kleinwort[12], G. Knies[12], T. Köhler[1], J.H. Köhne[27], H. Kolanoski[3], F. Kole[8], S.D. Kolya[23], V. Korbel[12], M. Korn[9], P. Kostka[36], S.K. Kotelnikov[26], T. Krämerkämper[9], M.W. Krasny[7,30], H. Krehbiel[12], D. Krücker[2], U. Krüger[12], U. Krüner-Marquis[12], H. Küster[22], M. Kuhlen[27], T. Kurča[36], J. Kurzhöfer[9], D. Lacour[30], B. Laforge[10], R. Lander[8], M.P.J. Landon[21], W. Lange[36], U. Langenegger[37], J.-F. Laporte[10], A. Lebedev[26], F. Lehner[12], C. Leverenz[12], S. Levonian[26], Ch. Ley[2], G. Lindström[13], M. Lindstroem[22], J. Link[8], F. Linsel[12], J. Lipinski[14], B. List[12], G. Lobo[28], H. Lohmander[22], J.W. Lomas[23], G.C. Lopez[13], V. Lubimov[25], D. Lüke[9,12], N. Magnussen[35], E. Malinovski[26], S. Mani[8], R. Maraček[18], P. Marage[5], J. Marks[24], R. Marshall[23], J. Martens[35], G. Martin[14], R. Martin[20], H.-U. Martyn[1], J. Martyniak[7], T. Mavroidis[21], S.J. Maxfield[20], S.J. McMahon[20], A. Mehta[6], K. Meier[16], T. Merz[36], A. Meyer[14], A. Meyer[12], H. Meyer[35], J. Meyer[12], P.-O. Meyer[2], A. Migliori[29], S. Mikocki[7], D. Milstead[20], J. Moeck[27], F. Moreau[29], J.V. Morris[6], E. Mroczko[7],

D. Müller[38], G. Müller[12], K. Müller[12], P. Murín[18], V. Nagovizin[25], R. Nahnhauer[36], B. Naroska[14], Th. Naumann[36], P.R. Newman[4], D. Newton[19], D. Neyret[30], H.K. Nguyen[30], T.C. Nicholls[4], F. Niebergall[14], C. Niebuhr[12], Ch. Niedzballa[1], H. Niggli[37], R. Nisius[1], G. Nowak[7], G.W. Noyes[6], M. Nyberg-Werther[22], M. Oakden[20], H. Oberlack[27], U. Obrock[9], J.E. Olsson[12], D. Ozerov[25], P. Palmen[2], E. Panaro[12], A. Panitch[5], C. Pascaud[28], G.D. Patel[20], H. Pawletta[2], E. Peppel[36], E. Perez[10], J.P. Phillips[20], A. Pieuchot[24], D. Pitzl[37], G. Pope[8], S. Prell[12], R. Prosi[12], K. Rabbertz[1], G. Rädel[12], F. Raupach[1], P. Reimer[31], S. Reinshagen[12], H. Rick[9], V. Riech[13], J. Riedlberger[37], F. Riepenhausen[2], S. Riess[14], E. Rizvi[21], S.M. Robertson[4], P. Robmann[38], H.E. Roloff[36], R. Roosen[5], K. Rosenbauer[1], A. Rostovtsev[25], F. Rouse[8], C. Royon[10], K. Rüter[27], S. Rusakov[26], K. Rybicki[7], N. Sahlmann[2], D.P.C. Sankey[6], P. Schacht[27], S. Schiek[14], S. Schleif[16], P. Schleper[15], W. von Schlippe[21], D. Schmidt[35], G. Schmidt[14], A. Schöning[12], V. Schröder[12], E. Schuhmann[27], B. Schwab[15], F. Sefkow[12], M. Seidel[13], R. Sell[12], A. Semenov[25], V. Shekelyan[12], I. Sheviakov[26], L.N. Shtarkov[26], G. Siegmon[17], U. Siewert[17], Y. Sirois[29], I.O. Skillicorn[11], P. Smirnov[26], J.R. Smith[8], V. Solochenko[25], Y. Soloviev[26], A. Specka[29], J. Spiekermann[9], S. Spielman[29], H. Spitzer[14], F. Squinabol[28], R. Starosta[1], M. Steenbock[14], P. Steffen[12], R. Steinberg[2], H. Steiner[12,40], B. Stella[33], A. Stellberger[16], J. Stier[12], J. Stiewe[16], U. Stößlein[36], K. Stolze[36], U. Straumann[38], W. Struczinski[2], J.P. Sutton[4], S. Tapprogge[16], M. Taševský[32], V. Tchernyshov[25], S. Tchetchelnitski[25], J. Theissen[2], C. Thiebaux[29], G. Thompson[21], P. Truöl[38], J. Turnau[7], J. Tutas[15], P. Uelkes[2], A. Usik[26], S. Valkár[32], A. Valkárová[32], C. Vallée[24], D. Vandenplas[29], P. Van Esch[5], P. Van Mechelen[5], Y. Vazdik[26], P. Verrecchia[10], G. Villet[10], K. Wacker[9], A. Wagener[2], M. Wagener[34], A. Walther[9], B. Waugh[23], G. Weber[14], M. Weber[12], D. Wegener[9], A. Wegner[27], T. Wengler[15], M. Werner[15], L.R. West[4], T. Wilksen[12], S. Willard[8], M. Winde[36], G.-G. Winter[12], C. Wittek[14], E. Wünsch[12], J. Žáček[32], D. Zarbock[13], Z. Zhang[28], A. Zhokin[25], M. Zimmer[12], F. Zomer[28], J. Zsembery[10], K. Zuber[16], and M. zurNedden[38]

[1] I. Physikalisches Institut der RWTH, Aachen, Germany[a]

[2] III. Physikalisches Institut der RWTH, Aachen, Germany[a]

[3] Institut für Physik, Humboldt-Universität, Berlin, Germany[a]

[4] School of Physics and Space Research, University of Birmingham, Birmingham, UK[b]

[5] Inter-University Institute for High Energies ULB-VUB, Brussels; Universitaire Instelling Antwerpen, Wilrijk; Belgium[c]

[6] Rutherford Appleton Laboratory, Chilton, Didcot, UK[b]

[7] Institute for Nuclear Physics, Cracow, Poland[d]

[8] Physics Department and IIRPA, University of California, Davis, California, USA[e]

[9] Institut für Physik, Universität Dortmund, Dortmund, Germany[a]

[10] CEA, DSM/DAPNIA, CE-Saclay, Gif-sur-Yvette, France

[11] Department of Physics and Astronomy, University of Glasgow, Glasgow, UK[b]

[12] DESY, Hamburg, Germany[a]

[13] I. Institut für Experimentalphysik, Universität Hamburg, Hamburg, Germany[a]

[14] II. Institut für Experimentalphysik, Universität Hamburg, Hamburg, Germany[a]

[15] Physikalisches Institut, Universität Heidelberg, Heidelberg, Germany[a]

[16] Institut für Hochenergiephysik, Universität Heidelberg, Heidelberg, Germany[a]

[17] Institut für Reine und Angewandte Kernphysik, Universität Kiel, Kiel, Germany[a]

[18] Institute of Experimental Physics, Slovak Academy of Sciences, Košice, Slovak Republic[f]
[19] School of Physics and Chemistry, University of Lancaster, Lancaster, UK[b]
[20] Department of Physics, University of Liverpool, Liverpool, UK[b]
[21] Queen Mary and Westfield College, London, UK[b]
[22] Physics Department, University of Lund, Lund, Sweden[g]
[23] Physics Department, University of Manchester, Manchester, UK[b]
[24] CPPM, Université d'Aix-Marseille II, IN2P3-CNRS, Marseille, France
[25] Institute for Theoretical and Experimental Physics, Moscow, Russia
[26] Lebedev Physical Institute, Moscow, Russia[f]
[27] Max-Planck-Institut für Physik, München, Germany[a]
[28] LAL, Université de Paris-Sud, IN2P3-CNRS, Orsay, France
[29] LPNHE, Ecole Polytechnique, IN2P3-CNRS, Palaiseau, France
[30] LPNHE, Universités Paris VI and VII, IN2P3-CNRS, Paris, France
[31] Institute of Physics, Czech Academy of Sciences, Praha, Czech Republic[f,h]
[32] Nuclear Center, Charles University, Praha, Czech Republic[f,h]
[33] INFN Roma and Dipartimento di Fisica, Universita "La Sapienza", Roma, Italy
[34] Paul Scherrer Institut, Villigen, Switzerland
[35] Fachbereich Physik, Bergische Universität Gesamthochschule Wuppertal, Wuppertal, Germany[a]
[36] DESY, Institut für Hochenergiephysik, Zeuthen, Germany[a]
[37] Institut für Teilchenphysik, ETH, Zürich, Switzerland[i]
[38] Physik-Institut der Universität Zürich, Zürich, Switzerland[i]
[39] Visitor from Yerevan Phys. Inst., Armenia
[40] On leave from LBL, Berkeley, USA
[a] Supported by the Bundesministerium für Forschung und Technologie, FRG, under contract numbers 6AC17P, 6AC47P, 6DO57I, 6HH17P, 6HH27I, 6HD17I, 6HD27I, 6KI17P, 6MP17I, and 6WT87P
[b] Supported by the UK Particle Physics and Astronomy Research Council, and formerly by the UK Science and Engineering Research Council
[c] Supported by FNRS-NFWO, IISN-IIKW
[d] Supported by the Polish State Committee for Scientific Research, grant nos. 115/E-743/SPUB/P03/109/95 and 2 P03B 244 08p01, and Stiftung für Deutsch-Polnische Zusammenarbeit, project no.506/92
[e] Supported in part by USDOE grant DE F603 91ER40674
[f] Supported by the Deutsche Forschungsgemeinschaft
[g] Supported by the Swedish Natural Science Research Council
[h] Supported by GA ČR, grant no. 202/93/2423, GA AV ČR, grant no. 19095 and GA UK, grant no. 342
[i] Supported by the Swiss National Science Foundation

1 Introduction

The study of elastic production of vector mesons in photo- and leptoproduction (Fig. 1a) in fixed target experiments has provided information on the hadronic component of the photon and on the nature of diffraction.

With the advent of the electron-proton collider HERA, there is renewed interest in vector meson production, in particular at large Q^2 (Q^2 is minus the square of the exchanged photon four-momentum). HERA experiments have observed in deep-inelastic scattering that the proton structure function F_2 increases rapidly [1] with increasing W, the $\gamma^* p$ invariant mass, which is in striking contrast with the slow rise of the total γp cross section at $Q^2 \simeq 0$ [2]. In addition, the rise of F_2 already at relatively low Q^2 values ($Q^2 \lesssim 2$ GeV^2) indicates that the transition between these two behaviours is rapid [3]. The study of the elastic production of vector mesons is expected to provide useful information about these different regimes, and in particular about the transition between them.

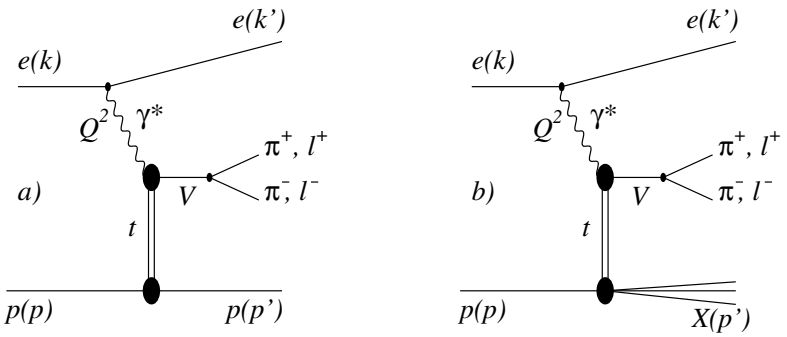

Figure 1: Diffractive vector meson production: a) elastic; b) proton dissociation.

The subject of this paper [4] is the study of elastic ϱ and J/ψ meson electroproduction at large Q^2 ($Q^2 > 8$ GeV^2) and high W ($\langle W \rangle \simeq 90$ GeV/c^2), in the reactions

$$e\ p \rightarrow e\ \varrho\ p;\ \varrho \rightarrow \pi^+\ \pi^-, \tag{1}$$

$$e\ p \rightarrow e\ J/\psi\ p;\ J/\psi \rightarrow l^+\ l^-;\ l = e \text{ or } \mu. \tag{2}$$

After the presentation of the event selection and of the mass distributions, the total cross sections and the differential distributions for reactions (1) and (2) are studied. Features relevant for the study of the transition regime are then discussed, in particular the energy dependence of the cross section, the t distribution (t is the square of the four-momentum transferred from the photon to the target), the vector meson polarisation, and the evolution of the J/ψ : ϱ cross section ratio. The results are discussed in the light of the interplay of hard and soft physics processes. Results on ϱ production in a similar kinematic range have been presented by the ZEUS Collaboration [5].

2 Models and phenomenology

The elastic production of light vector mesons, in particular of ϱ mesons, by real or quasi-real photons ($Q^2 \simeq 0$), a process called hereafter photoproduction, exhibits numerous

features typical of soft, hadron-like interactions. These are a small angle peak in the distribution of the vector meson scattering angle with respect to the incident photon beam direction ("elastic peak"), a steepening of this distribution with increasing energy ("shrinkage"), for $W \gtrsim 10$ GeV/c^2 a slow increase with energy of the cross section, and s-channel helicity conservation ($SCHC$).

These observations support the vector meson dominance model (VDM) [6, 7], according to which a photon with energy greater than a few GeV behaves predominantly as the superposition of the lightest (ϱ, ω, ϕ) $J^{PC} = 1^{--}$ mesons. In this framework, the cross section for elastic vector meson production is related to the total meson$-$proton cross section through the optical theorem, and the energy dependence is related to the "universal" energy dependence of the total hadron$-$proton cross section. Neglecting a contribution ("reggeon exchange") which decreases with energy approximately as $s^{-0.5}$, the latter is parameterised at high energy as $\sigma_{tot} \propto s^{\delta}$ with $\delta \simeq 0.0808$, $\sqrt{s}$ being the hadron$-$proton centre of mass energy [8]. This is expressed in Regge theory as due to soft pomeron exchange. The elastic production of ϱ mesons has been studied extensively by fixed target experiments in photoproduction [7, 9], for intermediate Q^2 [10] and for $Q^2 \gtrsim 6$ GeV^2 [11]. Also at HERA, the photoproduction of ϱ mesons exhibits the characteristic features of soft interactions [12].

In contrast, the VDM approach does not give a satisfactory description of J/ψ photoproduction data [13, 14, 15]: the cross section is smaller than the VDM prediction (see [16]) and it increases significantly faster with energy than expected from soft pomeron exchange. This is also observed by the HERA experiments [17].

Using the hard scale provided by the mass of the charm quark, the fast increase of the J/ψ photoproduction cross section was predicted in the framework of QCD by Ryskin [18]. In his model, the interaction between the proton and the $c\bar{c}$ pair in the photon is mediated by a gluon ladder, and non-perturbative effects are included in the nucleon parton distribution.

At high energy and high Q^2, ϱ meson production is modelled using two different approaches based on QCD, which both refer to the pomeron as basically a two gluon system (see [19]). The ϱ meson production is thus related to the gluon distribution in the proton, but the two approaches emphasize respectively soft or hard behaviour.

In the soft model initially proposed by Donnachie and Landshoff [20, 21, 16], the gluons are described non-perturbatively and the elastic cross section is expected to increase slowly with energy: $d\sigma/dt\ (t = 0) \propto W^{4\delta}$, with $\delta \simeq 0.0808$. The vector mesons are predicted to be mostly longitudinally polarised, the $\gamma^* p$ cross section to fall as Q^{-6} and the J/ψ cross section to be comparable to that of the ϱ.

In the second approach, perturbative QCD calculations similar to the work of Ryskin have been performed by several groups [22, 23, 24], a hard scale being provided by the photon virtuality. A major prediction of this model is a rapid increase of the cross section with W, as a consequence of the rise of the gluon distribution in the proton. It is stressed, however, that non-perturbative processes are also expected to be present in an intermediate energy region [22, 25]. The scattering amplitude is obtained in these calculations from the convolution of the hadronic wave function of the photon, of the scattering amplitude of this hadronic component, and of the final state vector meson wave function. This is because the photon is viewed at sufficient energy as the coherent superposition of

hadronic states formed well before the target (essentially $q\bar{q}$ pairs), whereas the final state meson is formed beyond it, the corresponding time scales being much longer than the interaction time. As a consequence, the spatial dimensions of the hadronic wave function are an essential parameter in the interplay of perturbative and non-perturbative effects. It is predicted that the hard effects should show up earlier for small size objects than for large ones, and for longitudinally than for transversely polarised photons. The Q^2 dependence of the $\gamma^* p$ cross section is predicted, as in the non-perturbative approach, to fall as Q^{-6} but when the evolution of the parton distribution and quark Fermi motion are taken into account, it was pointed out that the Q^2 distribution is expected to be harder [25]. In view of the more compact J/ψ wave function, the J/ψ : ϱ cross section ratio has been predicted [25] to exceed, at very high energy, the value 8 : 9 obtained from SU(4) and the quark counting rule [26].

In addition to these two "microscopic" approaches inspired by QCD, calculations are also performed for elastic vector meson production on the basis of multiple pomeron exchange, with the effective pomeron intercept depending on the photon virtuality [27]. A stronger increase of the cross section with energy is again predicted than for soft pomeron exchange with $\delta \simeq 0.0808$.

3 Detector and event selection

The data presented here correspond to an integrated luminosity of 2.8 pb^{-1} for the ϱ and 3.1 pb^{-1} for the J/ψ mesons. They were collected in 1994 using the H1 detector. HERA was operated with 27.5 GeV positrons and 820 GeV protons[1]. The detector is described in detail in ref. [28].

The event final state corresponding to reactions (1) and (2) consists of the scattered positron and two particles of opposite charges, originating from a vertex situated in the nominal e^+p interaction region. In most cases, the scattered proton remains inside the beam pipe because of the small momentum transfer to the target in elastic interactions.

In the Q^2 range studied here, the positron is identified as an electromagnetic cluster with an energy larger than 12 GeV, reconstructed in the backward electromagnetic calorimeter (BEMC) and associated with a hit in the proportional chamber (BPC) placed in front of it at 141 cm from the nominal interaction vertex[2]. The BEMC covers the polar angles $151^\circ < \theta < 176^\circ$. Its electromagnetic energy resolution is $\sigma_E/E \simeq 6 - 7\%$ in the energy range of the positrons selected for the present studies. The BPC angular acceptance is $155.5^\circ < \theta < 174.5^\circ$. The scattered positron polar angle θ_e is determined from the positions of the BPC hit and of the interaction vertex. The trigger used for the present analyses requires the presence of a total energy larger than 10 GeV deposited in the BEMC, outside a square of 32×32 cm^2 around the beam pipe. Additional cuts, similar to those used for the structure function analysis [1a], are applied to the hit and cluster position and shape in order to provide high trigger efficiency and good quality

[1] For the ϱ studies only positron data are used, whereas the small amount of data taken with e^-p scattering is included in the J/ψ sample; in this report, *positrons* refers both to positrons and electrons.

[2] The forward ($+z$) direction, with respect to which polar angles are measured, is defined as that of the incident proton beam, the backward direction is that of the positron beam.

positron measurement. These cuts are complemented by the selection of events with Q^2 > 8 GeV^2.

The decay pions (ϱ events) or leptons (J/ψ events) are detected in the central tracking detector, consisting mainly of two coaxial cylindrical drift chambers, 2.2 m long and respectively of 0.5 and 1 m outer radius. The charged particle momentum component transverse to the beam direction is measured in these chambers by the track curvature in the 1.15 T magnetic field generated by the superconducting solenoid which surrounds the inner detector, with the field lines directed along the beam axis. Two polygonal drift chambers with wires perpendicular to the beam direction, located respectively at the inner radius of the two coaxial chambers, are used for a precise measurement of the particle polar angle. For the present analyses, two tracks with transverse momenta p_t larger than 0.1 GeV/c are required to be reconstructed in the central region of the tracker. For ϱ production, the polar angles must lie in the range $25^\circ < \theta < 155^\circ$, corresponding to particles completely crossing the inner cylindrical drift chamber for interactions at the nominal vertex position. For J/ψ production, the accepted range is extended to $20^\circ < \theta < 160^\circ$ in order to increase the statistics as much as possible while keeping good detection efficiency. The vertex position is reconstructed using these tracks. No other track linked to the interaction vertex is allowed in the tracking detector, except possibly the positron track. To suppress beam-gas interactions, the vertex must be reconstructed within 30 cm of the nominal interaction point in z, which corresponds to 3 times the width of the vertex distribution. In addition, the accepted events are restricted to the range $40 < W < 140$ GeV/c^2 for ϱ mesons and $30 < W < 150$ GeV/c^2 for J/ψ mesons.

The tracking detector is surrounded by a liquid argon calorimeter situated inside the solenoid and covering the polar angular range $4^\circ < \theta < 153^\circ$ with full azimuthal coverage. In the case of elastic interactions, the calorimeters should register only activity associated with the decay particles or the positron. However, due to noise in the calorimeters and to the small pile-up from different events, elastic ϱ and J/ψ production can be accompanied by the presence of additional energy clusters. These are considered in terms of the variable E_{max}, defined as the energy of the most energetic cluster which is not associated with a track. The E_{max} distribution shows a peak at small values, attributed mostly to elastic and diffractive interactions, and a broad maximum at higher energies. The cut $E_{max} < 1$ GeV is applied to enhance exclusive ϱ production. This is discussed in section 5, together with the effect of the cut $|t| < 0.5$ GeV^2.

The sample of events containing a positron and a vector meson candidate includes two main contributions: elastic production (see Fig. 1a), defined by reactions (1) and (2), and events where the proton is diffractively excited into a system X of mass M_X, which subsequently dissociates (Fig. 1b). Non-resonant background is also present. It is possible to identify most of the "proton dissociation" events with the components of the H1 detector placed in the forward region [29], namely the forward part of the liquid argon calorimeter $4^\circ \leq \theta \leq 10^\circ$, the forward muon detectors (arrays of muon chambers placed around the beam pipe in the proton direction, $3^\circ \leq \theta \leq 17^\circ$) and the proton remnant tagger (an array of scintillators placed 24 m downstream of the interaction point, $0.06^\circ \leq \theta \leq 0.17^\circ$). When particles from the diffractively excited system interact in the beam pipe and the collimators, the interaction products can be detected in these forward detectors. The events are tagged as due to proton dissociation by the presence of a

cluster with energy E_{fw}^{LAr} larger than 1 GeV (0.75 GeV for the J/ψ candidates) at an angle $\theta_{fw}^{LAr} < 10°$ in the liquid argon calorimeter, or by at least 2 pairs of hits in the forward muon detectors (one hit pair is compatible with noise), or by at least one hit in the proton remnant tagger. This last criterion is not used for the J/ψ events, since they have a flatter t distribution than the ϱ events and would be partially vetoed by the proton tagger.

In order to minimise the effects of QED radiation in the initial state, the difference between the total energy and the total longitudinal momentum $E - p_z$ of the positron and the two particles emitted in the central part of the detector is required to be larger than 45 GeV. If no particle, in particular a radiated photon, has escaped detection in the backward direction, $E - p_z$ should be twice the incident positron energy, i.e. 55 GeV.

The selection criteria for the two samples, supplemented by the mass selections discussed in section 5, are summarised in Table 1.

	ϱ	J/ψ
positron selection	em. cluster > 10 GeV in BEMC outside 32×32 cm^2 reconstructed positron energy > 12 GeV associated BPC hit $Q^2 > 8$ GeV^2	
VM reconstruction	2 tracks fitting to vertex (+ possibly e^+) $p_t > 0.1$ GeV/c	
	$25° < \theta_{track} < 155°$	$20° < \theta_{track} < 160°$
	$40 < W < 140$ GeV/c^2	$30 < W < 150$ GeV/c^2
background suppression	$\lvert z_{vertex} - z_{nom.} \rvert < 30$ cm	
	$E_{max} < 1$ GeV	–
	$\lvert t \rvert < 0.5$ GeV^2	–
p. dissoc. ev. tagging	$E_{fw}^{LAr} < 1$ GeV for $\theta_{fw}^{LAr} < 10°$	$E_{fw}^{LAr} < 0.75$ GeV for $\theta_{fw}^{LAr} < 10°$
	≤ 1 hit pair in forward muon detectors	
	no hit in proton tagger	–
radiative corrections	$E - p_z > 45$ GeV	
mass selection	$0.6 < m_{\pi^+\pi^-} < 1.0$ GeV/c^2	$2.8 < m_{l^+l^-} < 3.4$ GeV/c^2
selected sample	180 events	31 events

Table 1: Selection criteria for ϱ and J/ψ events.

4 Kinematics and cross section definitions

The kinematics of reactions (1) and (2) are described with the variables commonly used for deep-inelastic interactions. In addition to s (the square of the e^+p centre of mass energy), Q^2 and W, it is useful to define the two Bjorken variables $y = p \cdot q / p \cdot k$ (in the proton rest frame, the energy fraction transferred from the positron to the hadrons) and $x = Q^2/2p \cdot q$, where k, p, q are, respectively, the four-momenta of the incident positron,

of the incident proton and of the virtual photon. These variables[3] obey the relations $Q^2 = xys$ and $W^2 = Q^2\ (\frac{1}{x} - 1)$.

The kinematical variables can be reconstructed from four measured quantities: the energies and the polar angles of the scattered positron and of the vector meson. With the "double angle" method [30] used for the present analyses, Q^2 and y are computed using the polar angles θ and γ of the positron and of the vector meson, which are well measured:

$$Q^2 = 4E_0^2\ \frac{\sin\gamma\ (1+\cos\theta)}{\sin\gamma + \sin\theta - \sin(\gamma+\theta)}, \tag{3}$$

$$y = \frac{\sin\theta\ (1-\cos\gamma)}{\sin\gamma + \sin\theta - \sin(\gamma+\theta)}, \tag{4}$$

where E_0 is the energy of the incident positron.

The meson momentum components are obtained from the measured decay products. The momentum of the scattered positron is computed from Q^2 and y, which provides better precision than the direct measurement. The energy transfer to the proton being negligible, the absolute value of t is given by:

$$|t| \simeq (\vec{p}_{tp})^2 = (\vec{p}_{te} + \vec{p}_{tv})^2, \tag{5}$$

where $\vec{p}_{tp}$, $\vec{p}_{te}$ and $\vec{p}_{tv}$ are, respectively, the momentum components transverse to the beam direction of the final state proton, positron and vector meson[4].

The fourth quantity which is directly measured, the positron energy, is used to compute the variable $E - p_z$:

$$E - p_z = (E_e + E_v) - (p_{ze} + p_{zv}), \tag{6}$$

E_e and E_v being the energies of the scattered positron and of the vector meson, and p_{ze} and p_{zv} their momentum components parallel to the beam direction.

The cross section for elastic electroproduction of a vector meson V can be converted into a $\gamma^* p$ cross section using the relation

$$\frac{d^2\sigma_{tot}(ep \to eVp)}{dy\ dQ^2} = \Gamma\ \sigma_{tot}(\gamma^* p \to Vp) = \ \Gamma\ \sigma_T(\gamma^* p \to Vp)\ (1 + \varepsilon\ R), \tag{7}$$

where σ_{tot}, σ_T and σ_L are the total, transverse and longitudinal $\gamma^* p$ cross sections,

$$R\ = \sigma_L/\sigma_T, \tag{8}$$

and Γ is the flux of transverse virtual photons given by

$$\Gamma = \frac{\alpha_{em}\ (1 - y + y^2/2)}{\pi\ y\ Q^2}; \tag{9}$$

ε is the polarisation parameter

$$\varepsilon = \frac{1-y}{1 - y + y^2/2}. \tag{10}$$

[3] In this paper, the positron and proton masses are neglected.

[4] The lowest $|t|$ value kinematically allowed, $t_{min} \simeq (Q^2 + m_V^2)^2\ m_p^2\ /y^2 s^2$, is negligible in this experiment.

Information on the vector meson production process can be obtained from the angular distributions of the decay particles. In particular, the probability r_{00}^{04} for the ϱ meson to be longitudinally polarised can be determined from the distribution of $\cos\theta^*$, where θ^* is the angle, in the ϱ rest frame, between the direction of the positively charged decay pion and the ϱ direction in the $\gamma^* p$ centre of mass system (helicity frame) [7, 31]:

$$\frac{\mathrm{d}N}{\mathrm{d}\cos\theta^*} \propto 1 - r_{00}^{04} + (3\ r_{00}^{04} - 1)\ \cos^2\theta^*. \tag{11}$$

With the assumption of s-channel helicity conservation ($SCHC$), r_{00}^{04} is related to R:

$$R = \frac{1}{\varepsilon}\ \frac{r_{00}^{04}}{1 - r_{00}^{04}}. \tag{12}$$

5 Mass distributions and final samples

Fig. 2a shows for the selected events (Table 1) the distribution of the invariant mass $m_{\pi^+\pi^-}$ in the range $m_{\pi^+\pi^-} < 2$ GeV/c^2, obtained by assigning the pion mass to the particles detected in the central tracker. The mass distribution without the E_{max} and t cuts (insert in Fig. 2a) is seen to peak at small $m_{\pi^+\pi^-}$ values. The E_{max} cut strongly reduces the background of events containing neutral particles, and enhances the ϱ peak. The t cut is very effective in rejecting non-resonant events containing, in addition to the ϱ candidate and the positron, particle(s) with a significant transverse momentum, which is not used to compute $\vec{p}_{tp}$ in eq. (5). This cut also enhances the elastic production signal compared to the background of proton dissociation events, which are known to have a flatter t distribution. In total, 180 events are found in the ϱ peak region with $0.6 < m_{\pi^+\pi^-} < 1.0$ GeV/c^2.

In Fig. 2a, events compatible with the ϕ mass, when the charged particles detected in the central tracker are considered as kaons, have been removed ($m_{K^+K^-} < 1.04$ GeV/c^2). Assuming that vector mesons are produced according to the quark counting rule with the SU(3) ratios $\varrho : \omega : \phi = 9 : 1 : 2$, the Monte Carlo simulation described below indicates that the remaining ϕ and ω reflections contribute, in the $m_{\pi^+\pi^-}$ range $(0.4 - 0.6)$ GeV/c^2, 2.0% of the ϱ signal in the peak, and 0.7% in the range $(0.6 - 1.0)$ GeV/c^2. These contributions were subtracted statistically.

The $m_{\pi^+\pi^-}$ distribution is described by a relativistic Breit-Wigner function, over a non-resonant background attributed to incompletely reconstructed diffractive photon dissociation. The Breit-Wigner function has the form [32]

$$\frac{dN(m_{\pi\pi})}{dm_{\pi\pi}} = \frac{m_{\pi\pi}\ m_\rho\ \Gamma(m_{\pi\pi})}{(m_\rho^2 - m_{\pi\pi}^2)^2 + m_\rho^2\ \Gamma^2(m_{\pi\pi})}, \tag{13}$$

with $\Gamma(m_{\pi\pi})$ the mass dependent width

$$\Gamma(m_{\pi\pi}) = \Gamma_\rho\ (\frac{q^*}{q_0^*})^3\ \frac{2}{1 + (q^*/q_0^*)^2}. \tag{14}$$

Here m_ρ is the ϱ resonance mass and Γ_ρ the width; q^* is the pion momentum in the $(\pi^+\pi^-)$ rest frame, and q_0^* this momentum when $m_{\pi^+\pi^-} = m_\rho$.

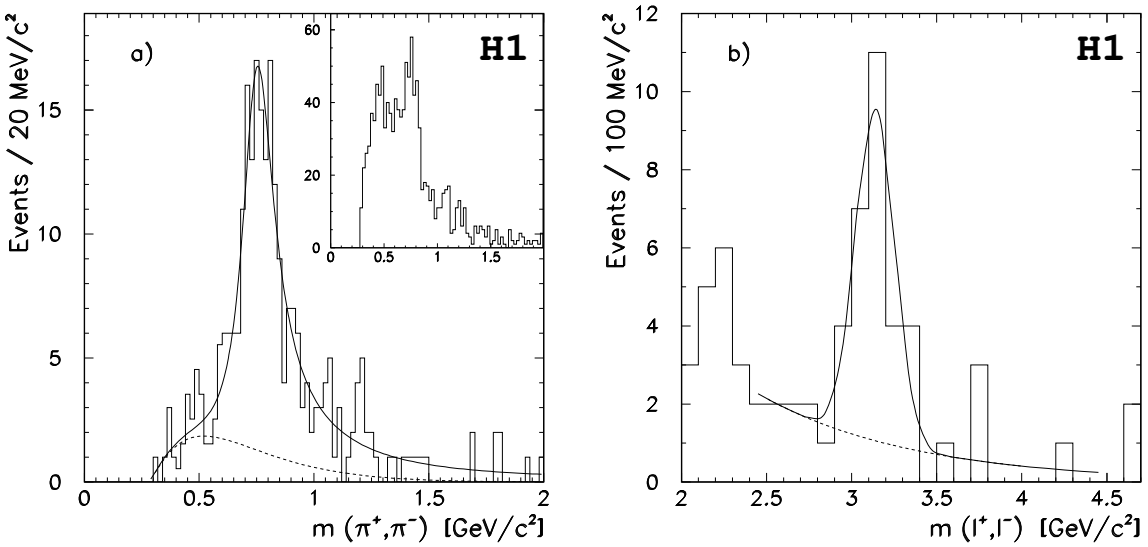

Figure 2: a) $m_{\pi^+\pi^-}$ mass distribution for the events with $Q^2 > 8$ GeV^2, $40 < W < 140$ GeV/c^2, $|t| < 0.5$ GeV^2, $E_{max} < 1$ GeV and no proton dissociation signal in the forward detectors; the superimposed curve is the result of a fit to a relativistic Breit-Wigner distribution over the background (15), which is described by the dashed curve. In the insert: same distribution without the E_{max} and t cuts; b) $m_{l^+l^-}$ mass distribution for the events with $Q^2 > 8$ GeV^2, $30 < W < 150$ GeV/c^2 and no proton dissociation signal in the forward detectors; the superimposed curve is the result of a fit to a Gaussian distribution over an exponential background in the range $2.4 < m_{l^+l^-} < 4.5$ GeV/c^2.

The background has been parameterised using the distribution

$$\frac{dN(m_{\pi\pi})}{dm_{\pi\pi}} = \alpha_1 \ (m_{\pi\pi} - 2m_\pi)^{\alpha_2} \ e^{-\alpha_3 m_{\pi\pi}}, \tag{15}$$

where m_π is the pion mass and α_1, α_2 and α_3 are free parameters. This form, which includes a two pion threshold and an exponential fall off, is in qualitative agreement with the background shape in the insert of Fig. 2a.

With these parameterisations, the resonance mass is 763 ± 10 MeV/c^2 and the width is 176 ± 23 MeV/c^2, in agreement with the Particle Data Group (PDG) values of 770 and 151 MeV/c^2 [33]. No skewing to low values of $m_{\pi^+\pi^-}$ is needed to describe the ϱ shape (for the Ross-Stodolsky parameterisation [34], the skewing exponent is found to be $n = 0.3 \pm 0.5$).

Two alternative forms have been used for the resonance width:

$$\Gamma(m_{\pi\pi}) = \Gamma_\rho \ (\frac{q^*}{q_0^*})^3 \ \frac{m_\rho}{m_{\pi\pi}} \tag{16}$$

and

$$\Gamma(m_{\pi\pi}) = \Gamma_\rho \ (\frac{q^*}{q_0^*})^3. \tag{17}$$

They also give a ϱ meson mass and width compatible with the PDG data.

The non-resonant background under the ϱ peak is estimated to be 11 $\pm$ 6%. The error includes the uncertainty on the resonance parameterisation and on the background shape, estimated by using for the latter an alternative linearly decreasing form.

The distribution of the invariant mass $m_{l^+l^-}$ for the selected events in the J/ψ region is presented in Fig. 2b. The J/ψ mass is 3.13 ± 0.03 GeV/c^2. The peak width is slightly larger than, but compatible with, the expectation obtained from the detector simulation. No t selection is applied since the t distribution is significantly flatter than for the ϱ mesons (see Fig. 3). No E_{max} cut is required in view of the small background in this high mass region (compare Fig. 2b and insert in Fig. 2a): all J/ψ candidate events have E_{max} < 1.35 GeV, of which 4 have E_{max} larger than 1 GeV.

A sample of 31 J/ψ candidate events is thus selected with the cut $|m_{l^+l^-} - m_\psi|$ < 300 MeV/c^2, where m_ψ is the J/ψ meson mass. The non-resonant background is estimated by fitting the sidebands using an exponential distribution and amounts to roughly 20% (6.8 events). No lepton identification is required, but 10 of the J/ψ candidate events contain two identified electrons and 7 contain two identified muons.

One event with $E_{max} > 1$ GeV is a $\psi' \to J/\psi\pi^0\pi^0$ candidate, with one identified muon and neutral clusters detected in the electromagnetic part of the liquid argon calorimeter, attributed to the interaction of photons from π^0 meson decay. The measured J/ψ mass is 3.16 ± 0.04 GeV/c^2. The invariant mass computed using the two charged tracks and the neutral clusters is 3.67 ± 0.09 GeV/c^2, in excellent agreement with the Particle Data Group value (3.69 GeV/c^2) [33].

Kinematical characteristics of the selected events are summarised in Table 2.

	ϱ	J/ψ
$\langle Q^2 \rangle$ [GeV^2]	13.4 ± 0.4	17.7 ± 1.5
$\langle W \rangle$ [GeV/c^2]	81 ± 2	92 ± 6
$\langle$scattered e^+ energy$\rangle$[GeV]	25.5 ± 0.1	24.9 ± 0.3
$\langle$scattered e^+ $p_t\rangle$ [GeV/c]	3.4 ± 0.1	3.9 ± 0.2
$\langle$meson energy$\rangle$ [GeV]	4.2 ± 0.1	6.0 ± 0.3
$\langle$track $p_t\rangle$ [GeV/c]	1.7 ± 0.1	2.3 ± 0.2

Table 2: Averages of kinematical variables characterising the selected events.

6 Corrections and simulations

Table 3 summarises the correction factors applied to the selected samples to take account of detector acceptance and efficiencies, smearing effects, losses due to the selection criteria and remaining backgrounds.

Most corrections are estimated using a Monte Carlo simulation based on the vector meson dominance model, which permits variation of the Q^2, W and t dependences, as

well as of the value of R [35]. The H1 detector response is simulated in detail, and the events are subjected to the same reconstruction and analysis chain as the data.

The accuracies of the ϱ (J/ψ) variable measurements are for W, 3.3 (4.3) GeV/c^2, for Q^2, 0.4 (0.4) GeV^2, for t, 0.06 (0.10) GeV^2. The values of the t slopes are little affected by the detector resolution.

The scattered positron selection criteria induce Q^2 dependent losses for $Q^2 \leq 12$ GeV^2. The error quoted in Table 3 corresponds to a systematic uncertainty on the positron direction of 2 mrad. The charged track selection criteria induce W dependent losses for small and high W, depending on the accepted W range in the two selections. A $Q^2 - W$ correlation of the losses is observed, and taken into account in the corrections. The correction for the t cut in the ϱ sample is computed using the measured t slope (see section 7.2).

	ϱ	J/ψ
trigger	1.01 ± 0.02	
positron acceptance (Q^2 dep.)	1.16 ± 0.03	1.15 ± 0.03
BPC hit $-$ cluster link	1.03 ± 0.02	
tracker acceptance (W dep.)	1.07 ± 0.01	1.29 ± 0.03
track reconstr. (per track)	1.05 ± 0.03	1.03 ± 0.03
track p_{tmin} (per track)	1.02 ± 0.01	1.00 ± 0.01
$\|t\|$ cut	1.03 ± 0.02	$-$
$E - p_z$ cut	1.02 ± 0.01	1.01 ± 0.01
E_{max} cut	1.03 ± 0.03	$-$
forward det. cuts ($\|t\|$ dep.)	1.04 ± 0.02	1.03 ± 0.03
mass selection	1.22 ± 0.01	1.00 ± 0.02
non-resonant background	0.89 ± 0.06	0.78 ± 0.14
proton dissoc. background	0.91 ± 0.08	0.75 ± 0.11
ϕ and ω background	0.99 ± 0.01	$-$
photon flux / bin integration	1.00 ± 0.04	1.00 ± 0.07
radiative corrections	0.96 ± 0.03	1.00 ± 0.04
luminosity	1.00 ± 0.02	

Table 3: Correction factors and systematic errors, averaged over the data samples.

The choice of the E_{max} cut for the ϱ sample is a compromise between the loss of elastic events to which a cluster is accidentally associated in the calorimeter, and the presence of non-resonant background in the final sample. The loss is estimated using a Monte Carlo simulation which includes random noise in the calorimeters superimposed on elastic events.

A simulation indicates that 2% of the elastic ϱ events with $|t| < 0.5$ GeV^2 are lost because the proton has acquired sufficient $\vec{p}_t$ to interact in the beam pipe walls, giving interaction products which are registered in the proton tagger; this loss is thus t dependent. For the J/ψ sample, 1.5% of the events are lost because of interaction products registered

in the forward muon detectors. Another 2% loss for both samples is due to spurious hits in the latter.

In view of the uncertainty on the high mass shape of the resonance, the ϱ cross section is quoted in this paper for $m_{\pi^+\pi^-} < 1.5$ GeV/c^2, i.e. $\simeq m_\rho + 5\ \Gamma_\rho$. The uncertainty is larger in the present case than for low energy data, for which a natural cut off is imposed by the limited available energy. With this definition of ϱ resonance production line shape, the correction for the mass selection $0.6 < m_{\pi^+\pi^-} < 1.0$ GeV/c^2 is respectively 21% and 23% for parameterisations (14) and (16).

A simulation was performed in order to estimate the contribution to the final samples of proton dissociation events which are not tagged by the forward detectors. The distribution of the target mass M_X is parameterised as $1/M_X^2$. High mass states are assumed to decay according to the Lund string model [36] or, alternatively, to a final state with particle multiplicity following the KNO scaling law and isotropic phase space distribution. In the resonance domain, the mass distribution follows measurements from p dissociation on deuterium [37] and resonance decays are described according to their known branching ratios. The decay particles are followed through the beam pipe walls and the forward detectors.

For the ϱ sample, the correction factor for the contamination of undetected proton dissociation events in the selected ϱ sample is 0.91 ± 0.08. This number is obtained from the number of measured events tagged and not tagged by the forward detectors, and from the detection probabilities provided by the Monte Carlo simulation. No assumption needs to be made for the ratio of proton dissociation to elastic events. The error is a conservative estimate taking into account the uncertainties on the efficiencies of the forward detectors for tagging proton dissociation events and on the dissociation model.

The correction factor for unobserved proton dissociation background in the selected J/ψ sample, for which the proton tagger is not used, is 0.75 ± 0.11.

The cross section measurements are given in the QED Born approximation for electron interactions. The effects of higher order processes are estimated using the HERACLES 4.4 generator [38].

Radiative corrections for the ϱ sample are of the order of 4% after the cut $E - p_z > 45$ GeV, and are weakly dependent on Q^2 and W. A systematic error of 3% is obtained by varying the effective Q^2 dependence of the $\gamma^* p$ cross section from Q^{-4} to Q^{-6} and by modifying the W dependence from a constant to a linearly increasing form[5]. The small value of the correction is due to the high $E - p_z$ cut resulting from the good BEMC resolution; for the chosen value of the cut, small smearing effects are observed.

For the J/ψ sample, the radiative corrections determined using the measured Q^2 and W dependences of the cross section vary from +2% to −2%.

[5] In practice, the input to the program is an effective "F_2 structure function" parameterisation, with the chosen Q^2 and W dependences of the ep cross section for vector meson production.

7 Results

7.1 Electroproduction cross sections

The ϱ and J/ψ data are grouped in several (Q^2, W) bins. Table 4 gives, for each bin, the number of events, the integrated ep cross section and the $\gamma^* p$ cross section obtained using relation (7) for a given (Q_0^2, W_0) value, taking into account the observed dependence across the bin. All known smearing, acceptance and background effects are corrected for. For the ϱ sample, each event is weighted using the differential flux factor given by eq. (9). A 4% systematic error accounts for the uncertainty in the Q^2 and W dependences of the cross section used for the bin size integration and the bin centre correction. For the J/ψ sample, in view of the small statistics, the photon flux is integrated over each (Q^2,W) bin. Since the data span a large range in Q^2 and W, this leads to a systematic error on the cross section of the order of 7%.

The integrated cross section for ϱ meson electroproduction with $m_{\pi^+\pi^-} < 1.5$ GeV/c^2 is

$$\sigma(e\ p \rightarrow e\ \varrho\ p) = 96 \pm 7\ (stat.) \pm 13\ (syst.)\ \text{pb}, \tag{18}$$

for $Q^2 > 8$ GeV^2 and $40 < W < 140$ GeV/c^2.

The cross section for J/ψ meson electroproduction, taking into account the $J/\psi \rightarrow 2$ leptons branching fraction 0.12 [33], is

$$\sigma(e\ p \rightarrow e\ J/\psi\ p) = 100 \pm 20\ (stat.) \pm 20\ (syst.)\ \text{pb}, \tag{19}$$

for $Q^2 > 8$ GeV^2 and $30 < W < 150$ GeV/c^2.

The ratio $J/\psi : \varrho$ is 0.64 ± 0.13 for $Q^2 = 10$ GeV^2 and 1.3 ± 0.5 for $Q^2 = 20$ GeV^2.

7.2 Momentum transfer distributions

The t distributions of the selected ϱ and J/ψ events (Fig. 3) show the forward exponential peaking $\propto e^{bt}$ characteristic of elastic interactions.

For the ϱ sample, the slope b of the t distribution is computed taking into account the contributions of the non-resonant and proton dissociation backgrounds estimated in sections 5 and 6. Their exponential slopes were taken to be respectively 0.15 ± 0.10 and 2.5 ± 1.0 GeV^{-2}, which is consistent with the t dependence of event samples which approximate these contributions. The results quoted below are rather insensitive to the choice of these slopes. The t distribution is corrected for detector effects, including the loss of elastic events tagged by the forward detectors.

A fit for $|t| < 0.6$ GeV^2 gives for the elastic slope the value $b = 7.0 \pm 0.8 \pm 0.4 \pm 0.5$ GeV^{-2} ($\chi^2 = 9.6$ /10 d.o.f.) for $Q^2 > 8$ GeV^2 and $40 < W < 140$ GeV/c^2. The first error corresponds to the statistical precision of the fit. The second describes the spread of the fits according to the choice of the $|t|$ range (0.4 to 0.6 GeV^2) and of the E_{max} cut value. The third comes from the uncertainties in the sizes and shapes of the backgrounds; it is dominated by the error on the total contribution of the non-resonant background. The t slope measured by the ZEUS Collaboration is $b = 5.1\ ^{+1.2}_{-0.9} \pm 1.0$ GeV^{-2} [5]. The values of the slopes for two Q^2 and two W domains are given in Table 5.

$e\ p \to e\ \varrho\ p$		
	$8 < Q^2 < 12$ GeV^2	
	$40 < W < 80$ GeV/c^2	$80 < W < 140$ GeV/c^2
number of events	57	47
total correction factor	1.53 ± 0.22	1.76 ± 0.25
integrated ep cross section [pb]	$31.5 \pm 4.2 \pm 4.5$	$29.8 \pm 4.3 \pm 4.2$
Q_0^2 [GeV^2], W_0 [GeV/c^2]	10, 65	10, 115
$\gamma^* p$ cross section [nb]	$25.8 \pm 3.4 \pm 3.7$	$29.4 \pm 4.3 \pm 4.2$
	$12 < Q^2 < 50$ GeV^2	
	$40 < W < 80$ GeV/c^2	$80 < W < 140$ GeV/c^2
number of events	39	37
total correction factor	1.32 ± 0.19	1.23 ± 0.18
integrated ep cross section [pb]	$18.5 \pm 3.0 \pm 2.7$	$16.3 \pm 2.7 \pm 2.4$
Q_0^2 [GeV^2], W_0 [GeV/c^2]	20, 65	20, 115
$\gamma^* p$ cross section [nb]	$5.0 \pm 0.8 \pm 0.7$	$5.0 \pm 0.8 \pm 0.7$
$e\ p \to e\ J/\psi\ p$		
	$8 < Q^2 < 40$ GeV^2	
	$30 < W < 90$ GeV/c^2	$90 < W < 150$ GeV/c^2
number of events	15	16
total correction factor	1.50 ± 0.27	0.92 ± 0.17
integrated ep cross section [pb]	$61 \pm 18 \pm 12$	$40 \pm 12 \pm 8$
Q_0^2 [GeV^2], W_0 [GeV/c^2]	16, 65	16, 115
$\gamma^* p$ cross section [nb]	$7.8 \pm 2.2 \pm 1.6$	$12.2 \pm 3.4 \pm 2.5$
	$30 < W < 150$ GeV/c^2	
	$8 < Q^2 < 12$ GeV^2	$12 < Q^2 < 40$ GeV^2
number of events	10	21
total correction factor	1.82 ± 0.33	0.90 ± 0.16
integrated ep cross section [pb]	$49 \pm 18 \pm 10$	$51 \pm 13 \pm 10$
Q_0^2 [GeV^2], W_0 [GeV/c^2]	10, 88	20, 88
$\gamma^* p$ cross section [nb]	$17.6 \pm 6.3 \pm 3.7$	$6.6 \pm 1.6 \pm 1.4$

Table 4: Numbers of events and cross sections for different Q^2 and W ranges, for ϱ and for J/ψ elastic production; the $\gamma^* p$ cross sections are given for $Q^2 = Q_0^2, W = W_0$.

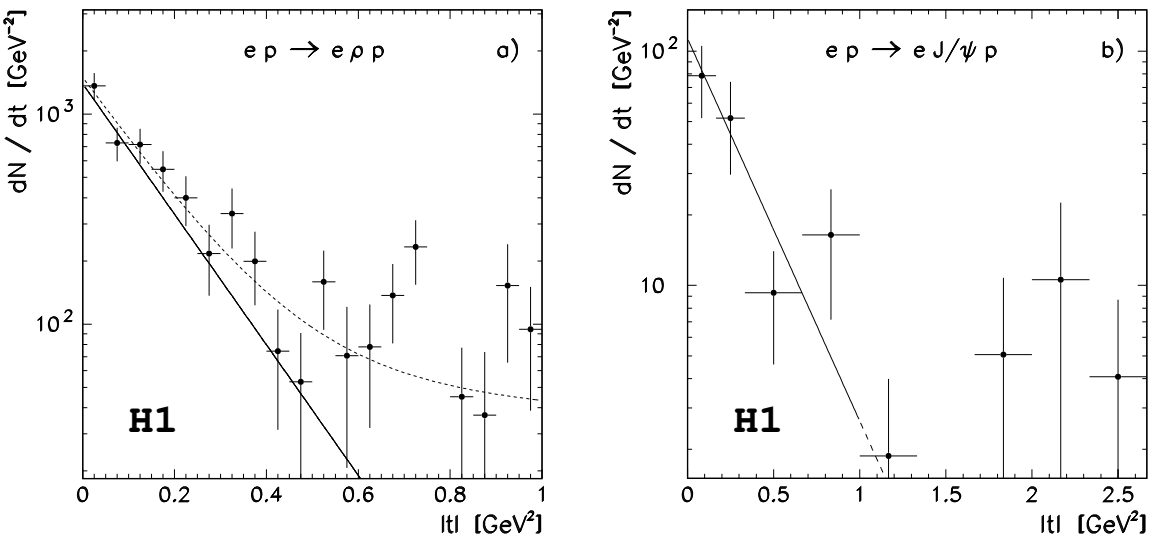

Figure 3: $|t|$ distributions for a) the ϱ sample; the data points are not corrected for background; the dashed line is the result of a fit taking the background into account, as described in the text; b) the J/ψ sample, corrected for the presence of background. Both distributions are corrected for acceptance, losses and smearing effects. The solid lines correspond to the elastic exponential slopes.

$40 < W < 140$ GeV/c^2	
$8 < Q^2 < 12$ GeV^2	$12 < Q^2 < 50$ GeV^2
$b = 7.8 \pm 1.0 \pm 0.7$ GeV^{-2}	$b = 5.7 \pm 1.3 \pm 0.7$ GeV^{-2}
$8 < Q^2 < 50$ GeV^2	
$40 < W < 80$ GeV/c^2	$80 < W < 140$ GeV/c^2
$b = 6.2 \pm 1.0 \pm 0.7$ GeV^{-2}	$b = 8.0 \pm 1.3 \pm 0.7$ GeV^{-2}

Table 5: Slopes of the ϱ meson t distributions for different Q^2 and W domains.

For the J/ψ sample, the slope value for $|t| < 1.0$ GeV^2 is $b = 3.8 \pm 1.2\ ^{+2.0}_{-1.6}$ GeV^{-2}, after subtraction of the proton dissociation and non-resonant backgrounds with slopes $b = 2$ GeV^{-2}. The systematic error is estimated by varying the background contributions by one standard deviation and their slopes between 0 and 3 GeV^{-2}. The combined value of the HERA experiments [17a-b] for the slope in photoproduction is $b = 4.0 \pm 1.0$ GeV^{-2}. Three events have $|t| > 1.1$ GeV^2 (see Fig. 3b), of which one has $E_{max} > 1$ GeV. These 3 events contribute 15% to the cross section quoted in this paper. The ψ' candidate event (see section 5) has $|t| = 0.16$ GeV^2, t being computed including the neutral clusters attributed to π^0 mesons ($Q^2 = 26.3$ GeV^2, $W = 72.6$ GeV/c^2).

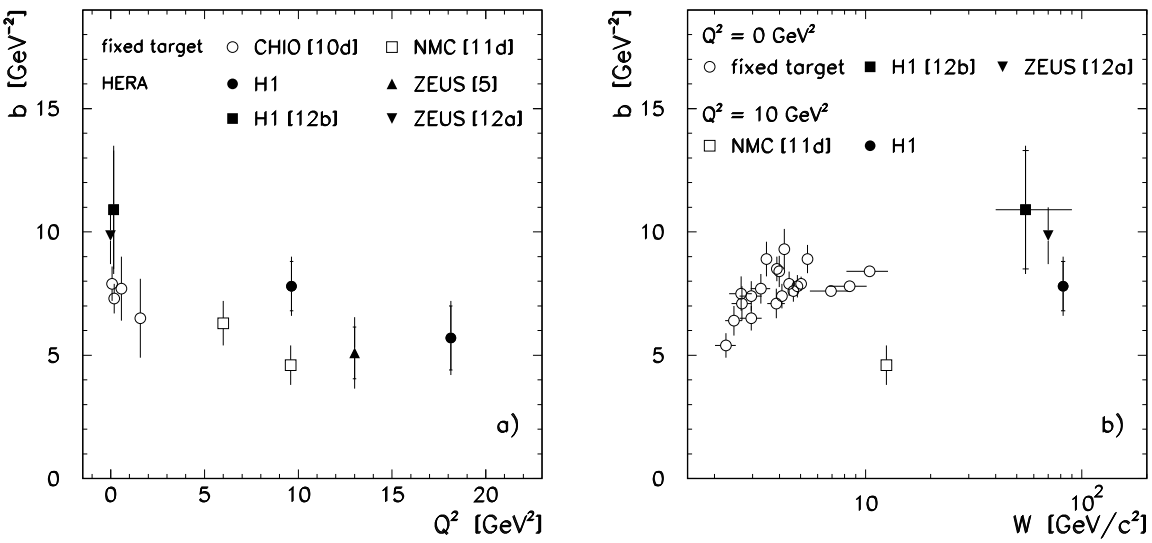

Figure 4: t slope for elastic ϱ production in fixed target and HERA experiments a) as a function of Q^2; b) as a function of W for photoproduction and for $Q^2 \simeq 10$ GeV^2.

Fig. 4a shows that for the W domain of the HERA experiments the decrease with rising Q^2 of the t slope for ϱ elastic production is similar to that observed at lower W.

The comparison of the NMC and H1 results for $Q^2 \simeq 10$ GeV^2 (Fig. 4b) shows an increase of the t slope with energy. This shrinkage of the elastic peak with W (or $\sqrt{s}$) is observed in diffractive hadron interactions [37] and in photoproduction (see the comparison of fixed target and HERA results in Fig. 4b). In the framework of Regge theory, for pomeron exchange and in terms of the exponential parameterisation, the shrinkage of the elastic peak can be written

$$b(W^2) = b(W^2 = W_0^2) + 2\ \alpha'\ \ln(W^2/W_0^2), \tag{20}$$

where α' is the slope of the effective pomeron Regge trajectory:

$$\alpha_{I\!P}(t) = \alpha_{I\!P}(0) + \alpha'\ t. \tag{21}$$

Applying relation (20) to the $Q^2 = 10$ GeV^2 results (with statistical and systematic errors combined quadratically) gives for α' the value 0.41 ± 0.18 GeV^{-2}, in agreement with a value of 0.25 GeV^{-2} deduced from hadronic interactions [39]. For the H1 data alone, there is also an indication for an increase of the slope with W (see Table 5).

7.3 Q^2 dependence of the cross sections

The Q^2 dependence of the total $\gamma^* p$ cross section ($\sigma_{tot} = \sigma_T + \varepsilon\,\sigma_L$) for the elastic ϱ meson production by virtual photons (Fig. 5a) can be described by Q^{-2n} with $n = 2.5 \pm 0.5 \pm 0.2$. In extracting the dependence on Q^2 of the cross section, correction has been made for the presence of non-resonant background, for which $n = 1.5 \pm 0.2$ as obtained from the events with $|t| > 0.5$ GeV^2 or $E_{max} > 1$ GeV. The second error on n reflects the uncertainty on the background size and shape and the spread of the results according to the details of the fitting procedure. The cross section dependence for the present data is close to that obtained by NMC ($n = 2.02 \pm 0.07$) and by ZEUS ($n = 2.1 \pm 0.4\ ^{+0.7}_{-0.3}$ for $0.0014 < x < 0.004$). It should be noted, however, that the NMC data span a large range in the polarisation parameter ε from $\varepsilon = 0.50$ at $Q^2 = 2.5$ GeV^2 to $\varepsilon = 0.80$ for $Q^2 > 10$ GeV^2, whereas the HERA data are for $\varepsilon = 0.99$. Although the Q^2 dependence is probably sensitive to this kinematical effect, it was not taken into account because the evolution of R with Q^2 in the NMC data (see eq. 7) is not published. The differences in the absolute normalisations are discussed in section 7.4.

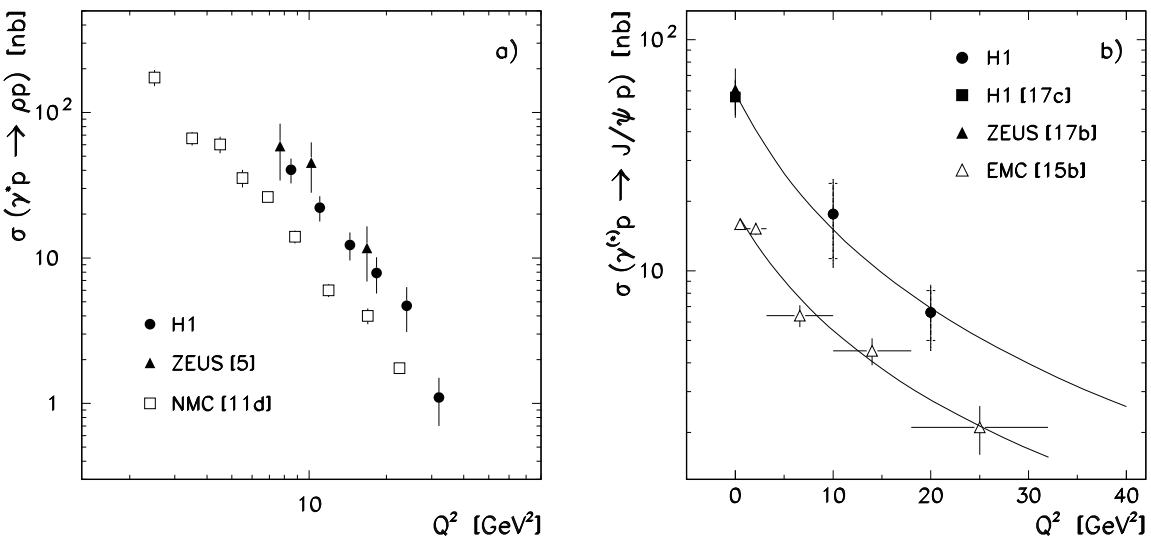

Figure 5: Q^2 dependence of the $\gamma^{(*)} p \to Vp$ cross section a) for ϱ production, the ZEUS points being given for the restricted x range $0.0014 < x < 0.004$; b) for J/ψ production[6], the curves being the result of the fits described in the text.

The Q^2 dependence of the J/ψ production cross section at HERA is shown in Fig. 5b. The errors on the high Q^2 data points include the uncertainty in the Q^2 dependence of the background. The evolution from photoproduction to high Q^2 is well described by $1\ /\ (Q^2 + m_\psi^2)^n$ with $n = 1.9 \pm 0.3$ ($stat.$). This is similar to the Q^2 dependence of the low energy EMC results [15], for which a fit of the data shown in Fig. 5b gives $n = 1.7 \pm 0.1$.

7.4 W dependence of the cross sections

The W dependence of the ϱ (for $m_{\pi^+\pi^-} < 1.5$ GeV/c^2) and J/ψ production cross sections is shown on Fig. 6 for $Q^2 = 10$ and 20 GeV^2. These values are chosen in order to minimise the bin centre corrections for the ϱ analysis.

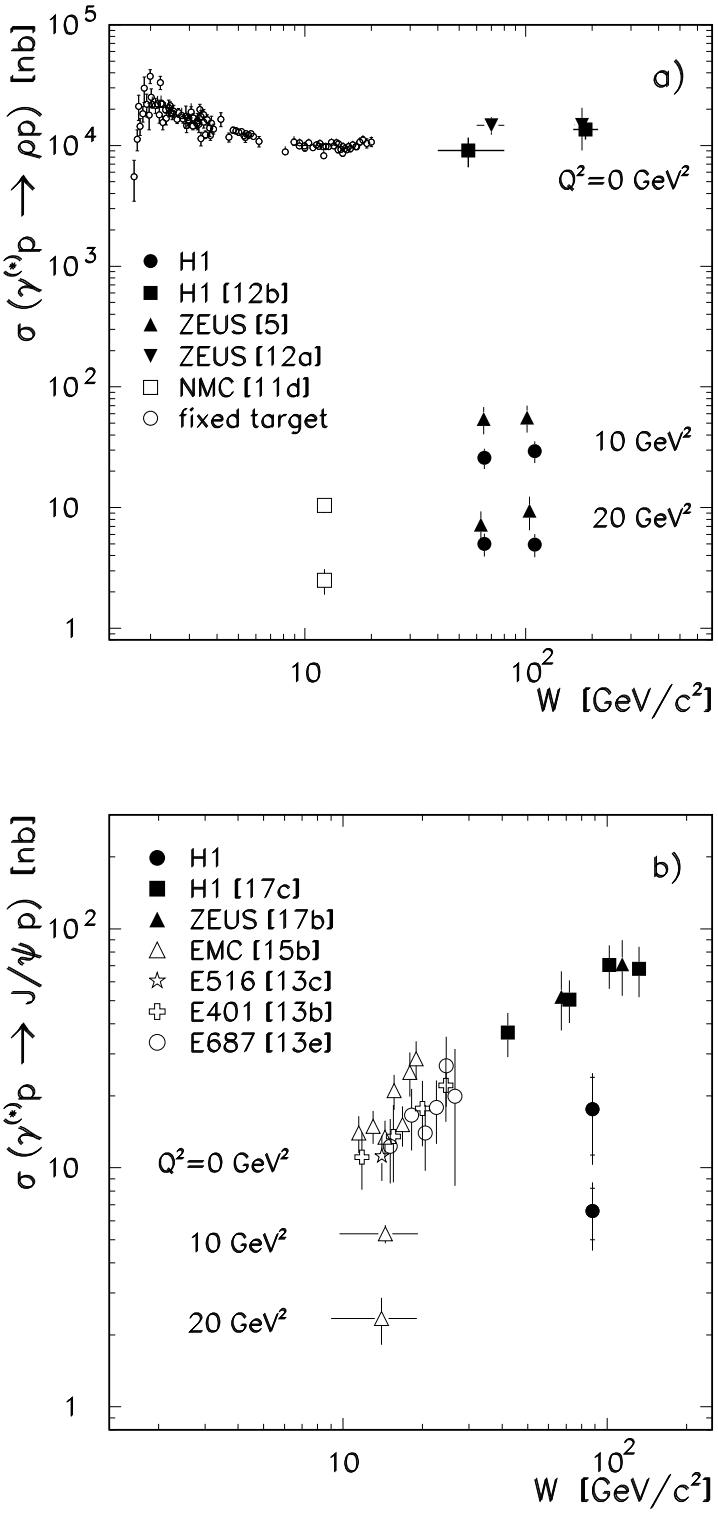

Figure 6: W dependence of the $\gamma^{(*)}\ p \to\ V\ p$ cross section in fixed target and HERA experiments a) for ϱ production (computed for $m_{\pi^+\pi^-} < 1.5$ GeV/c^2); b) for J/ψ production. For the ϱ data, an overall normalisation uncertainty of 31% for ZEUS and of 20% for NMC is not included in the plot.

The ZEUS results in Fig. 6a have been scaled to the Q^2 values of the H1 measurements using the dependence of the latter (see section 7.3). These results can be directly compared to the H1 results although they include no explicit cut-off on the $m_{\pi^+\pi^-}$ mass. Indeed, the cross sections quoted in [5] are determined assuming a non-relativistic Breit-Wigner mass distribution with mass independent width, integrated over the full kinematical range. It turns out that this procedure leads to a cross section closely similar to that obtained using the relativistic form of eq. (13-14) for $m_{\pi^+\pi^-} < 1.5$ GeV/c^2, as is done in the present experiment. The ZEUS results are higher than those of H1, but the discrepancy is not very significant when the overall 31% systematic error on the ZEUS results [5], which is not included in the plot, is taken into account. Other differences between the results of the two experiments are observed: both the ZEUS t (section 7.2) and $\cos\theta^*$ distributions (section 7.5) are flatter than for H1. It is worth emphasizing in this context that the event by event selection in the H1 analysis, which uses the forward detectors, provides a very clean elastic ϱ sample.

The NMC results shown in Fig. 6a are obtained from the published Q^2 dependence of the cross section for interactions on deuterium (Fig. 4 of [11d]), which has small nuclear corrections [40, 41]. They are corrected for the different values of the polarisation parameter ε in the two experiments (the NMC measurement of R is used). The published NMC cross section was computed using for the ϱ resonance the Breit-Wigner parameterisation given by eq. (13) and (16), for $m_{\pi^+\pi^-} < 1.5$ GeV/c^2 [40]. The results of the two experiments can thus be directly compared. An overall 20% systematic uncertainty [11d] is not included in the plot.

A significant increase with energy of the elastic $\gamma^* p$ cross section is observed from the NMC to the HERA domains. Following section 2, it is parameterised as $d\sigma/dt\ (t=0) \propto W^{4\delta}$. The fitted values of δ are for ϱ elastic production:

$$Q^2 = 10\ \text{GeV}^2 \ : \quad \delta = 0.14 \pm 0.05, \tag{22}$$

$$Q^2 = 20\ \text{GeV}^2 \ : \quad \delta = 0.10 \pm 0.06. \tag{23}$$

The errors result from the combination of statistical and systematic errors of both experiments, including the 20% normalisation uncertainty for NMC.

The measurements (22) and (23) take into account the following effects:

– the $d\sigma/dt\ (t=0)$ cross sections are obtained by multiplying the total cross sections by the corresponding b slopes. The H1 slopes given in Table 5 were used and the corresponding NMC slopes were computed[6] according to the shrinkage description given by eq. (20) with $\alpha' = 0.25\ \text{GeV}^{-2}$.

– the cross section definition[7] contains a kinematical factor due to phase space integration, involving the centre of mass energy W, the mass squared of the particles and Q^2. This factor is not part of the study of the interaction dynamics contained in the W evolution of the matrix element. As the Q^2 values considered here are rather large compared to W^2 for the NMC experiment and small for H1, there is a rising contribution to the W dependence amounting to 12% (26%) between NMC and H1 energies for $Q^2 = 10$

[6] For $Q^2 = 10$ GeV^2, the use of the measured NMC slope instead would lead to an additional increase of δ by 0.03. No measurement of the NMC slope is published for $Q^2 = 20$ GeV^2.

[7] See eq. (23.32) and (23.36), p. 1292 of [33].

(20) GeV^2. This corresponds to a decrease of δ by 0.02 (0.03), which is included in the measurements (22) and (23).

Additional effects may have to be taken into account:

– model predictions are often computed for the longitudinal cross section σ_L and not for the total cross section $\sigma_T + \varepsilon\ \sigma_L$. Taking into account the difference in the R values for the two experiments (see section 7.5), the δ values for σ_L alone would be increased by 0.02 with respect to the values (22) and (23) (a possible Q^2 dependence of R is not considered).

– at the NMC energies, reggeon exchange could contribute significantly to elastic ϱ production. Following the parameterisation obtained by Donnachie and Landshoff for the forward amplitude (eq. (9) of [16]) and assuming it holds for high Q^2, the contributions to the $d\sigma/dt$ ($t = 0$) cross sections of the purely reggeon exchange and of the reggeon−pomeron interference term are, respectively, 4% and 28% of the pomeron exchange contribution (0% and 4% at HERA). To extract the forward differential cross sections from the measured total cross sections, assumptions have to be made concerning the relevant b slopes. For the purely reggeon exchange term, the value 0.83 is used for the slope of the Regge trajectory [42], with the same parameter $b(W_0^2) = 2.5$ GeV^{-2} as for the pomeron ($W_0 = 1$ GeV/c^2). The slope for the interference term is chosen as the average of the pomeron and the reggeon slopes. When these contributions are subtracted, the value of δ is increased by 0.02.

Not including an error for theoretical uncertainties, the values of δ for σ_L and pomeron exchange only are 0.18 ± 0.05 for $Q^2 = 10$ GeV^2 and 0.14 ± 0.06 for $Q^2 = 20$ GeV^2.

The W dependence of J/ψ production is presented in Fig. 6b[8] for $Q^2 \simeq 0$, 10 and 20 GeV^2. A steep increase of the photoproduction cross section is observed from low energy to the HERA experiments. For higher Q^2 values, a similar increase is observed between the EMC and the H1 measurements. However, quantitative comparisons should be taken with caution in view of normalisation uncertainties and the possible presence of inelastic background in the fixed target data.

7.5 ϱ decay angular distribution

The acceptance corrected $\cos\theta^*$ distribution for the selected ϱ sample is shown in Fig. 7a. After subtraction of the non-resonant background, which is consistent with being flat in $\cos\theta^*$, and correction for detector effects, the fit of eq. (11) to this distribution gives $r_{00}^{04} = 0.73 \pm 0.05 \pm 0.02$. The first error is statistical, the second reflects the uncertainty on the background subtraction. Assuming $SCHC$, relation (12) gives $R = \sigma_L\ /\sigma_T = 2.7\ ^{+0.7}_{-0.5}\ ^{+0.3}_{-0.2}$, with $\langle\varepsilon\rangle = 0.99$.

The value of R is shown in Fig. 7b together with fixed target measurements[9] and given in Table 6 for two values of Q^2 and of W. Compared with results at low Q^2, a clear increase of R with Q^2 is observed.

An attempt was made to test the hypothesis [24] that the ϱ meson should be completely longitudinally polarised for $|t| \gg \Lambda^2_{QCD}$, by dividing the data with $|t| < 0.5$ GeV^2 into

[8] All results presented in Fig. 6b have been rescaled to take into account the latest measurements of the J/ψ branching fractions: $B(J/\psi \to e^+e^-) = 5.99 \pm 0.25\%$, $B(J/\psi \to \mu^+\mu^-) = 5.97 \pm 0.25\%$ [33].

[9] EMC measurements [11a] with largest errors have been omitted.

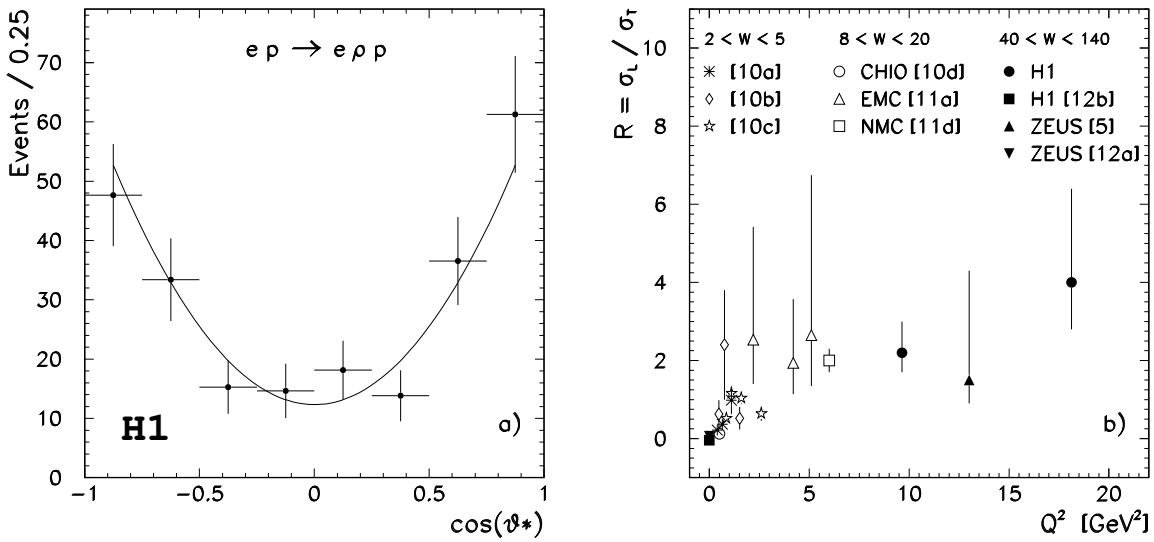

Figure 7: a) $\cos\theta^*$ distribution for the ϱ events, the superimposed curve being the result of a fit of eq. (11) to this distribution; b) Q^2 dependence of $R = \sigma_L\ /\sigma_T$ for ϱ elastic production, from several experiments.

$40 < W < 140$ GeV/c^2	
$8 < Q^2 < 12$ GeV^2	$12 < Q^2 < 50$ GeV^2
$R = 2.2\ ^{+0.8}_{-0.5}$	$R = 4.0\ ^{+2.4}_{-1.2}$
$8 < Q^2 < 50$ GeV^2	
$40 < W < 80$ GeV/c^2	$80 < W < 140$ GeV/c^2
$R = 2.2\ ^{+0.8}_{-0.5}$	$R = 3.7\ ^{+1.9}_{-1.1}$

Table 6: Values of $R = \sigma_L\ /\sigma_T$ for ϱ elastic production in different Q^2 and W domains.

two samples with $|t|$ respectively smaller and larger than 0.15 GeV^2. The predicted effect was not observed, but the imposed cut is probably too low to provide a sensitive test of the prediction.

8 Discussion and conclusions

The production of elastic ϱ and J/ψ mesons by virtual photons has been measured at HERA with the H1 detector. Samples of 180 and 31 events, respectively, have been collected with $Q^2 > 8$ GeV^2 and $40 < W < 140$ GeV/c^2 ($30 - 150$ GeV/c^2 for the J/ψ), for an integrated luminosity of 2.8 (3.1) pb^{-1}. Most of the proton dissociation background is removed using the forward components of the H1 detector and the small residual backgrounds are corrected for.

A major interest of the study of elastic vector meson production is that predictions have been proposed for the differential cross sections both in the framework of a soft, non-perturbative approach, and based on perturbative QCD calculations for hard processes.

The main difference between the predictions of the soft and of the hard approaches concerns the rise of the cross section with energy, expected respectively to be slow or fast. For ϱ production at high Q^2, the W dependence of the cross section attributed to pomeron exchange is parameterised as $d\sigma/dt\ (t = 0) \propto W^{4\delta}$. Using the NMC and the present H1 results, the measured values of δ for the total cross section $\sigma_T + \varepsilon\ \sigma_L$ are $\delta = 0.14 \pm 0.05$ for $Q^2 = 10$ GeV^2 and $\delta = 0.10 \pm 0.06$ for $Q^2 = 20$ GeV^2. For the longitudinal cross section σ_L alone, and taking into account possible reggeon exchange, these values would be $\delta = 0.18 \pm 0.05$ and $\delta = 0.14 \pm 0.06$, respectively.

For the soft pomeron model of Donnachie-Landshoff, the expected value is 0.08. For the hard approach, it is presumably in the range $0.20 - 0.25$ [3b]. The present measurements thus lie between the values expected for these two types of models.

The suggestion [23] that the ϱ cross section measurement may provide information on the gluon distribution in the proton is applicable only when the hard regime is reached. As this condition does not seem to be fulfilled for the present W and Q^2 ranges, an attempt to extract the gluon distribution from these data seems premature.

In contrast, the J/ψ production cross section for $Q^2 > 8$ GeV^2 increases strongly from the fixed target to the HERA region. This increase is of the same order as in photoproduction. This indicates that a hard regime is reached for J/ψ production already at low Q^2, which could be related to the smaller spatial extent of the wave function and the large scale provided by the charm quark mass.

A major result of the present measurement is the similarity of the cross sections for ϱ and J/ψ elastic production. Whereas J/ψ photoproduction, which is suppressed by factors of 100 to 1000 with respect to ϱ, is not well described by the "quark counting rule", quark flavour symmetry appears to be approximately restored for Q^2 of 10 to 20 GeV^2. Such a behaviour is expected both in the soft and the hard models. However, this evolution is observed to be faster than for some hard models (a ratio 1/2 has been proposed for $Q^2 \simeq 100$ GeV^2 [25]).

The t dependence of the production differential cross sections for ϱ and J/ψ mesons are found to be well described at low t values by exponential dependences e^{bt}. For the

ϱ sample, b is 7.0 ± 0.8 $(stat.) \pm 0.4$ $(syst.) \pm 0.5$ $(bg.)$ GeV^{-2}. This value is smaller than for photoproduction at HERA, showing that the decrease of the slope with rising Q^2 observed in fixed target experiments extends to the HERA regime. This behaviour can be attributed to the decrease of the $q\bar{q}$ transverse separation in the photon with rising Q^2.

The evolution of the slope with W is sensitive to the interplay of soft and hard effects in ϱ production. There is an indication that the shrinkage of the elastic peak observed in hadron interactions and ϱ photoproduction also occurs in the present electroproduction data, at large Q^2. This is as expected from Regge predictions based on soft pomeron exchange, in contrast with the little shrinkage predicted in perturbative calculations for hard processes [25].

For J/ψ production, the t distribution is well described with $b = 3.8 \pm 1.2 \, ^{+2.0}_{-1.6}$ GeV^{-2}, which is smaller than for the ϱ. This difference can be qualitatively explained by the fact that the J/ψ wave function is more compact than the ϱ wave function.

The Q^2 dependence of the ϱ total cross section can be described by a power law Q^{-2n}, with $n = 2.5 \pm 0.5 \pm 0.2$. This distribution is slightly harder than initially expected both for non-perturbative two gluon exchange and for hard QCD calculations ($\propto Q^{-6}$). It is compatible with predictions taking into account the Q^2 evolution of parton densities and the transverse motion of the quarks in the photon [25]. It should be noted that the calculations are performed for σ_L whereas the present measurement is of σ_{tot}, which includes a transverse contribution at the level of 20–25%, with presumably a steeper Q^2 dependence [22, 23].

The Q^2 dependence of the J/ψ production cross section is parameterised as $1/(Q^2 + m_\psi^2)^n$, with $n = 1.9 \pm 0.3$ $(stat.)$, which is similar to fixed target results.

The polar angle distribution of the decay pions indicates that ϱ mesons are mostly longitudinally polarised: the spin density matrix element r_{00}^{04} is $0.73 \pm 0.05 \pm 0.02$. Assuming *SCHC*, $R = \sigma_L / \sigma_T$ is $2.7 \, ^{+0.7}_{-0.5} \, ^{+0.3}_{-0.2}$. The increase of R with Q^2, which is predicted both by the non-perturbative model and the QCD calculations, is observed. The indication in the present data of an increase of R with W suggests, in the framework of hard physics, that perturbative features at high W and moderate Q^2 are indeed more important for longitudinal than for transverse photons.

In conclusion, the study of ϱ and J/ψ meson production offers a contrasting picture.

For J/ψ mesons, hard physics effects are probably at work already for very small Q^2. The present high Q^2 data support this interpretation, albeit with limited statistical precision.

For ϱ mesons, the W, t, Q^2 and $\cos\theta^*$ dependences of the cross section allow a more detailed study, from which a mixed picture emerges. It can be speculated that the present data correspond to a transition regime, with interplay of hard processes, amenable to perturbative description, and soft processes, requiring a non-perturbative approach. The W dependence of the cross section does not provide conclusive evidence in favour of a purely soft or a purely hard model. The indication of shrinkage of the elastic peak with W is important because it shows a continuation with increasing Q^2 of the photoproduction behaviour and is at variance with expectations for a purely hard behaviour. The observation that SU(4) flavour symmetry is restored in the J/ψ : ϱ cross section ratio, which is a striking feature of the present measurements, is expected in both models. The study of the Q^2 and $\cos\theta^*$ distributions also does not discriminate between the soft and hard

models, since their predictions are similar.

Acknowledgements

We are grateful to the HERA machine group whose outstanding efforts made this experiment possible. We appreciate the immense effort of the engineers and technicians who constructed and maintained the detector. We thank the funding agencies for their financial support of the experiment. We wish to thank the DESY directorate for the support and hospitality extended to the non-DESY members of the collaboration. We thank further J.-R. Cudell, B. Kopeliovich, A. Sandacz and H. Spiesberger for useful discussions.

References

[1] a. T. Ahmed et al., H1 Coll., *Nucl. Phys.* **B439** (1995) 471;
b. M. Derrick et al., ZEUS Coll., *Zeit. Phys.* **C65** (1995) 379.

[2] M. Derrick et al., ZEUS Coll., *Phys. Lett.* **B293** (1992) 465;
T. Ahmed et al., H1 Coll., *Phys. Lett.* **B299** (1993) 374;
M. Derrick et al., ZEUS Coll., *Zeit. Phys.* **C63** (1994) 391;
S. Aid et al., H1 Coll., *Zeit. Phys.* **C69** (1995) 27.

[3] a. M. Derrick et al., ZEUS Coll., *Measurement of the Proton Structure Function F_2 at low x and low Q^2 at HERA,* preprint DESY-95-193 (1995);
b. H1 Coll., *A measurement and QCD Analysis of the Proton Structure Function $F_2(x, Q^2)$ at HERA,* to be publ.

[4] Preliminary H1 results were presented at the Int. Europhys. Conf. on HEP, Brussels, 1995:
H1 Coll., *Exclusive ϱ^0 Production in Deep Inelastic Scattering Events at HERA*, EPS-0480;
H1 Coll., *J/ψ Meson Production in Deep Inelastic Scattering at HERA*, EPS-0469.

[5] M. Derrick et al., ZEUS Coll., *Phys. Lett.* **B356** (1995) 601.

[6] J.J. Sakurai, *Phys. Rev. Lett.* **22** (1969) 981;
J.J. Sakurai and D. Schildknecht, *Phys. Lett.* **B40** (1972) 121.

[7] T.H. Bauer et al., *Rev. Mod. Phys.* **50** (1978) 261, and references therein.

[8] A. Donnachie and P.V. Landshoff, *Phys. Lett.* **B296** (1992) 227.

[9] a. R.M. Egloff et al., *Phys. Rev. Lett.* **43** (1979) 657;
b. D. Aston et al., *Nucl. Phys.* **B209** (1982) 56.

[10] a. P. Joos et al., *Nucl. Phys.* **B113** (1976) 53;
b. C. del Papa et al., *Phys. Rev.* **D19** (1979) 1303;
c. D.G. Cassel et al., *Phys. Rev.* **D24** (1981) 2787;

d. W.D. Shambroom et al., CHIO Coll., *Phys. Rev.* **D26** (1982) 1;
e. B.Z. Kopeliovich and P. Marage, *Int. J. Mod. Phys.* **A8** (1993) 1513.

[11] a. J.J. Aubert et al., EMC Coll., *Phys. Lett.* **B161** (1985) 203;
b. J. Ashman et al., EMC Coll., *Zeit. Phys.* **C39** (1988) 169;
c. P. Amaudruz et al., NMC Coll., *Zeit. Phys.* **C54** (1992) 239;
d. M. Arneodo et al., NMC Coll., *Nucl. Phys.* **B429** (1994) 503.

[12] a. M. Derrick et al., ZEUS Coll., *Zeit. Phys.* **C69** (1995) 39;
b. S. Aid et al., H1 Coll., *Elastic Photoproduction of ϱ^0 Mesons at HERA,* preprint DESY-95-251 (1995), to be publ. in *Nucl. Phys.* **B**.

[13] a. U. Camerini et al., *Phys. Rev. Lett.* **35** (1975) 483;
b. M. Binkley et al., *Phys. Rev. Lett.* **48** (1982) 73;
c. B.H. Denby et al., *Phys. Rev. Lett.* **52** (1984) 795;
d. R. Barate et al., *Zeit. Phys.* **C33** (1987) 505;
e. P.L. Frabetti et al., *Phys. Lett.* **B316** (1993) 197.

[14] a. A.R. Clark et al., *Phys. Rev. Lett.* **43** (1979) 187; *Phys. Rev. Lett.* **45** (1980) 2092;
b. M. Arneodo et al., *Phys. Lett.* **B332** (1994) 195.

[15] a. J.J. Aubert et al., EMC Coll., *Phys. Lett.* **B89** (1980) 267;
b. J.J. Aubert et al., EMC Coll., *Nucl. Phys.* **B213** (1983) 1.

[16] A. Donnachie and P.V. Landshoff, *Phys. Lett.* **B348** (1995) 213.

[17] a. T. Ahmed et al., H1 Coll., *Phys. Lett.* **B338** (1994) 507;
b. M. Derrick et al., ZEUS Coll. *Phys. Lett.* **B350** (1995) 120;
c. H1 Coll., *Elastic and Inelastic Photoproduction of J/ψ Mesons at HERA,* preprint DESY-96-037 (1996).

[18] M.G. Ryskin, *Zeit. Phys.* **C57** (1993) 89.

[19] F.E. Low, *Phys. Rev.* **D12** (1975) 163;
S. Nussinov, *Phys. Rev. Lett.* **34** (1975) 1268.

[20] A. Donnachie and P.V. Landshoff, *Phys. Lett.* **B185** (1987) 403.

[21] J.R. Cudell, *Nucl. Phys.* **B336** (1990) 1.

[22] B.Z. Kopeliovich and B.G. Zakharov, *Phys. Rev.* **D44** (1991) 3466;
B.Z. Kopeliovich et al., *Phys. Lett.* **B324** (1994) 469;
J. Nemchik et al., *Phys. Lett.* **B341** (1994) 228.

[23] S.J. Brodsky et al., *Phys. Rev.* **D50** (1994) 3134.

[24] I.F. Ginzburg, D.Yu. Ivanov and V.G. Serbo, *Semihard diffractive production of neutral mesons by off shell photons and the range of pQCD validity,* preprint hep-ph/9508309 (1995).

[25] L. Frankfurt, W. Koepf and M. Strikman, *Hard diffractive electroproduction of vector mesons in QCD,* preprint TAUP-2290-95, hep-ph/9509311 (1995);
see also:
H. Abramowicz, L. Frankfurt and M. Strikman, *Interplay of Hard and Soft Physics in Small x Deep Inelastic Processes,* preprint DESY-95-047 (1995);
L. Frankfurt and M. Strikman, *QCD and Diffraction in DIS,* Talk given at the Workshop on DIS and QCD, Paris, April 1995, preprint hep-ph/9510291 (1995).

[26] E.M. Levin and L.L. Frankfurt, *JETP Lett.* (1965) 65;
H.J. Lipkin and F. Scheck, *Phys. Rev. Lett.* **169** (1966) 71.

[27] L.P.A. Haakman, A. Kaidalov and J.H. Koch, *Production of vector mesons by real and virtual photons at high energies,* preprint NIKHEF-95-033, hep-ph/9507394 (1995).

[28] I. Abt et al., H1 Coll., *The H1 detector,* preprint DESY-93-103 (1993).

[29] T. Ahmed et al., H1 Coll., *Phys. Lett.* **B348** (1995) 681.

[30] S. Bentvelsen, J. Engelen and P. Kooijman, *Reconstruction of (x, Q^2) and extraction of structure functions in neutral current scattering at HERA,* in: Proc. of the Workshop on Physics at HERA, ed. W. Buchmüller and G. Ingelman, Hamburg 1992, Vol. 1, p. 23;
K.C. Hoeger, *Measurement of x, y, Q^2 in Neutral Current Events,* ibid., p. 43.

[31] K. Schilling and G. Wolf, *Nucl. Phys.* **B61** (1973) 381.

[32] T.J. Jackson, *Nuovo Cim.* **34** (1964) 1644.

[33] L. Montanet et al., *Review of Particle Properties, Phys. Rev.* **D50** (1994) 1173.

[34] M. Ross and L. Stodolsky, *Phys. Rev.* **149** (1966) 1172.

[35] *DIFFVM program,* see: B. List, *Diploma Thesis*, Techn. Univ. Berlin, unpubl. (1993).

[36] T. Sjöstrand, *PYTHIA 5.7 and JETSET 7.4. Physics and Manual,* preprint CERN-TH.7112/93 (1993) (revised February 1994).

[37] K. Goulianos, *Phys. Rep.* **101** (1983) 169.

[38] H. Spiesberger, *HERACLES 4.4,* unpublished program manual (1993);
A. Kwiatkowski, H. Spiesberger and H.-J. Möhring, *An event generator for ep interactions at HERA including radiative processes,* in: Proc. of the Workshop on Physics at HERA, ed. W. Buchmüller and G. Ingelman, Hamburg 1992, Vol. 3, p. 1294.

[39] A. Donnachie and P.V. Landshoff, *Nucl. Phys.* **B267** (1986) 690.

[40] A. Sandacz, *private communication.*

[41] M. Arneodo et al., *Nuovo Cim.* **108A** (1995) 1247.

[42] J.-R. Cudell, K. Kang and S.K. Kim, *Simple pole fits to pp and $\bar{p}p$ total cross sections and real parts,* preprint SNUTP 95-103, Brown-HET-1016, ULG-PNT-95-1-JRC, (1996).